Journal of Materials Chemistry A

Core-Shell PdPb@Pd Aerogels with Multiply-Twinned Intermetallic Nanostructures: Facile Synthesis with Accelerated Gelation Kinetics and Their Enhanced Electrocatalytic Properties

Journal:	*Journal of Materials Chemistry A*
Manuscript ID	TA-COM-12-2017-011233.R4
Article Type:	Paper
Date Submitted by the Author:	19-Mar-2018
Complete List of Authors:	Zhu, Chengzhou; Washington State University, School of Mechanical and Material Engineering Shi, Qiurong; Washington State University, School of Mechanical and Materials Engineering Fu, Shaofang; Washington State University, School of Mechanical and Materials Engineering Song, Junhua; Washington State University, School of Mechanical and Materials Engineering Du, Dan; Washington State University, School of Mechanical and Materials Engineering; Central China Normal University, Department of Chemistry Su, Dong; Brookhaven National Laboratory, Center for Functional Nanomaterials Engelhard, Mark; Pacific Northwest National laboratory, Environmental Molecular Sciences Laboratory Lin, Yuehe; Pacific Northwest National Laboratory,

Journal Name

ARTICLE

Core-Shell PdPb@Pd Aerogels with Multiply-Twinned Intermetallic Nanostructures: Facile Synthesis with Accelerated Gelation Kinetics and Their Enhanced Electrocatalytic Properties

Received 00th January 20xx,
Accepted 00th January 20xx

DOI: 10.1039/x0xx00000x

www.rsc.org/

Chengzhou Zhu,[a,b] Qiurong Shi,[a] Shaofang Fu,[a] Junhua Song,[a] Dan Du,[a,b] Dong Su,*[c] Mark H. Engelhard,[d] and Yuehe Lin*[a]

Delicately engineering the well-defined noble metal aerogels with favorable structural and compositional features is of vital importance for wide applications. Here, we reported one-pot and facile method for synthesizing core-shell PdPb@Pd hydrogels/aerogels with multiply-twinned grains and ordered intermetallic phase using sodium hypophosphite as a multifunctional reducing agent. Due to the accelerated gelation kinetics induced by increased reaction temperature and specific function of sodium hypophosphite, the formation of hydrogels can be completed within 4 hrs. Owing to their unique porous structure and favorable geometric and electronic effects, the optimized PdPb@Pd aerogels exhibit enhanced electrochemical performance towards ethylene glycol oxidation with a mass activity of 5.8 times higher than Pd black.

Introduction

Rational synthesis and assembly of porous noble metal nanomaterials and construction of more functional architectures has seen much progress and enormous efforts have been directed toward the synthesis and exploration of them in catalysis, sensors, energy conversion and storage.[1-6] Among them, noble metal-involved aerogels, as a class of promising electrocatalysts, hold great promise in fuel cells and related fields.[7, 8] These noble metal aerogels are porous monoliths with controlled nanostructures, bridging the gap between nanoscale and macroscale. Due to the combined advantages of noble metals and aerogels, such as low density, high surface area, profuse porosity and excellent electrocatalytic activity, noble metal aerogels can not only significantly increase the number of active site of noble metals but also provide enhanced electrolyte permeability and fast mass transport/electron transfer, further accelerating the reaction kinetics. After the first report on the creation of noble metal aerogels such as Pt, Ag/Au and Ag/Pt,[9] the novel unsupported aerogels with a proper shape and composition control have shown excellent electrocatalysts for oxygen reduction reaction, ethanol/formic acid electrooxidation.[10-13]

The synthesis of noble-metal aerogels is of vital importance to control its morphology, porosity and other physical features. Besides the usual two-step gelation process featured with complicated concentration and destabilization steps,[9, 14, 15] one-step process utilizing the reduction of noble metal precursors with $NaBH_4$ provides a promising alternative for the facile synthesis of hydrogels/aerogels.[16, 17] Our recent progress for efficient synthesis of nonprecious metal-involved CuM (M=Pd, Pt and Au) aerogels within 6 hrs featured with accelerated gelation kinetics further enriches the synthetic methodology for noble metal hydrogels/aerogels and extending their electrochemical applications.[18] While tremendous efforts have been devoted to this emerging field, tuning their properties via the construction of a diverse variety of structures and compositions in nanostructures require the new synthetic systems and several critical issues on the design and synthesis of noble metal-based aerogels should be addressed. Normally, $NaBH_4$ was used as reducing agent in this one-step method. The resultant noble metal aerogels characterized by nanowire network structures were obtained irrespective of their compositions.[16-19] So far, as a key parameter, the effect of the reducing agents on the gelation of nanoparticles and the formation of the final hydrogels has not yet been investigated. Second, constructing nonprecious metals-involved bi/multimetallic aerogels along with a shape/structure-controlled poses a greater challenge for enhancing their electrocatalytic performance due to the

[a] School of Mechanical and Materials Engineering Washington State University, Pullman, WA 99164, USA. E-mail: yuehe.lin@wsu.edu
[b] Key Laboratory of Pesticide and Chemical Biology, Ministry of Education, College of Chemistry, Central China Normal University, Wuhan 430079, PR China
[c] Center for Functional Nanomaterials, Brookhaven National Laboratory, Upton, NY 11973, USA. E-mail: dsu@bnl.gov
[d] Environmental Molecular Science Laboratory, Pacific Northwest National Laboratory, Richland, WA 99354, USA.

Electronic Supplementary Information (ESI) available: Experimental details, digital pictures of Pd_3Pb_1@Pd hydrogel formation at different stages, TEM images of the Pd_1Pb_1@Pd, Pd_5Pb_1@Pd aerogels and Pd nanowire networks, XPS spectra of PdPb@Pd aerogels, TEM image of the PdPb hydrogel, solution color change upon addition of NaH_2PO_2 to the mixture of different noble metal precursors and $Pb(NO_3)_2$, TEM images of the PdCu aerogels. See DOI: 10.1039/x0xx00000x

synergistic effects in term of favorable geometric and electronic structures.[20] Furthermore, accelerating gelation kinetics and further shortening the gel formation time will be critical for the development of noble metal aerogels and their practical applications.

In this study, an one-pot method of synthesizing core-shell PdPb@Pd hydrogels/aerogels were developed for the first time using sodium hypophosphite as a multifunctional reducing agent. Besides, sodium hypophosphite also plays a critical role in affecting the structural evolution of the multiply-twinned PdPb@Pd aerogels with ordered intermetallic phase. By taking advantage of the accelerated gelation kinetics with the help of increased reaction temperature and specific function of sodium hypophosphite, the formation of this kind of hydrogel can be completed with 4 hrs. Thanks to the unique structures and favorable composition, the obtained multiply-twinned PdPb@Pd aerogels exhibited enhanced electrochemical performance towards ethylene glycol oxidation.

Results and discussion

The synthesis procedure of the multiply-twinned Pd_3Pb_1@Pd aerogels is illustrated in Fig. 1a. Typically, 0.315 mL Na_2PdCl_4 (0.05 M) and 0.105 mL $Pb(NO_3)_2$ (0.05 M) was dissolved with 35 mL of deionized water with stirring at 60 ° C. Then, 0.84 mL $NaHPO_2$ (0.5 M) was rapidly injected into the above solution (Table S1, ESI†). The resulting solution was stirred for 30 seconds, followed by settling for about 4 h. Different from previously reported, different reducing agent, i.e. $NaHPO_2$, rather than $NaBH_4$ was used in our reaction systems. It is found that solution turn black instantly upon the addition of $NaHPO_2$, indicating the reduction of metal precursors. Surprisingly, fluffy black solids start to appear in solution within 15 min, which was faster than most noble metal aerogels reported previously,[16-19] where $NaBH_4$ was adopted as reducing agent. As reaction time goes on, fluffy black solids fused and the jelly-like hydrogel is completely settled down in solution after 4 hrs (Fig. 1b and Fig. S1, ESI†). After carefully washing with water and completely replacing water with ethanol, the final

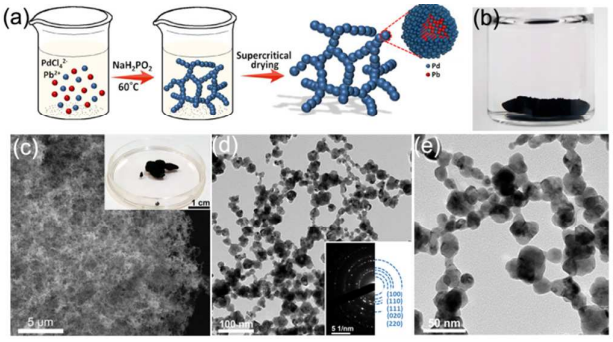

Fig. 1 (a) Schematic illustration of the synthesis of multiply-twinned PdPb@Pd aerogels. Digital pictures of the multiply-twinned Pd_3Pb_1@Pd hydrogels (b) and the resultant aerogels (Inset in (c)). SEM (c) and TEM (d, e) images of multiply-twinned Pd_3Pb_1@Pd aerogels. Inset in (d) shows a SAED pattern.

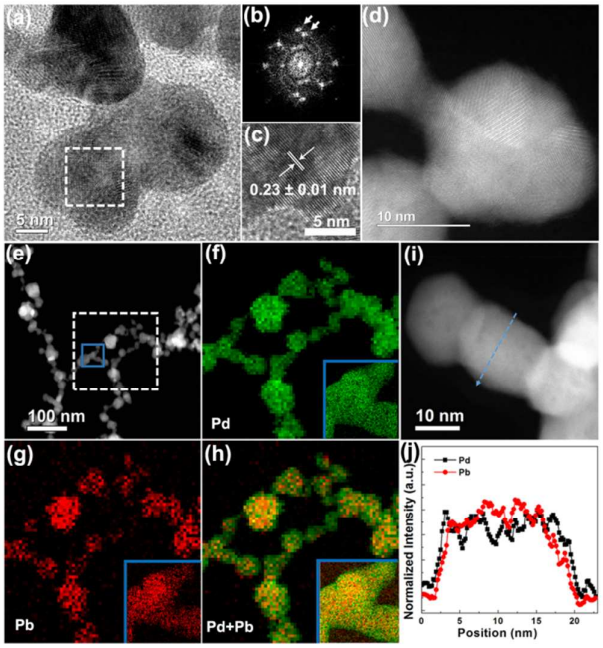

Fig. 2 HRTEM images (a, c) of multiply-twinned Pd_3Pb_1@Pd aerogels and corresponding FFT image (b) derived from the white square in Figure a. (d) HAADF-STEM image of PdPb@Pd aerogels. STEM-EELS elemental mapping (e-h) and line scan (i and j) result for Pd_3Pb_1@Pd aerogels.

aerogels can be obtained using supercritical CO_2 drying.

The obtained PdPb aerogels were characterized by scanning electron microscopy (SEM) and transmission electron microscopy (TEM). Different from carbon-based aerogels, metal aerogels are fragile and subject to break because of the lack of flexibility. SEM image revealed that the as-prepared Pd_3Pb_1@Pd aerogels possess porous nanostructures and are comprised of fused nanostructures. It should be noted that a common feature of the noble metal aerogels is that the building blocks involved, normally nanoparticles, are fused and interconnected with each other. As can be seen from the TEM images of Fig. 1d and e, the resultant Pd_3Pb_1@Pd aerogels were composed of fused nanoparticles with uneven size distribution of 5-40 nm, which is different from aforementioned noble metal-based aerogels characterized by distinct nanowire networks with a narrow size distribution of building blocks through one-step synthetic approach using $NaBH_4$ as reducing agent. The typical selected-area electron diffraction (SAED) pattern presented in the inset of Fig. 1d shows the presence of ordered intermetallic Pd_3Pb phase (JCPDS 20-0827) in Pd_3Pb_1@Pd aerogels.

To further characterize the atomic structure of the resultant aerogels, high-resolution TEM (HRTEM) and high-angle annular dark-field scanning TEM (HAADF-STEM) were carried out. As shown in Fig. 2a and d, the 5-fold twin boundaries are clearly observed in the fused nanoparticles within Pd_3Pb_1@Pd aerogel. The fast Fourier transform (FFT, Fig.2b) of the Pd_3Pb_1@Pd aerogel further confirms their multiply-twinned structures.[21, 22] The lattice spacings are measured to be 0.23 ± 0.01 nm,

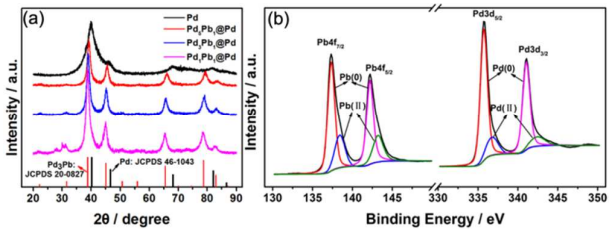

Fig. 3 (a) XRD patterns of PdPb@Pd aerogels with different compositions and a standard Pd pattern. (b) XPS of the Pb 4f and Pd 3d peaks of Pd_3Pb_1@Pd aerogel.

corresponding to the (111) plane of Pd_3Pb nanocrystal. The elemental distribution of Pd and Pb at the fused nanoparticles was characterized using STEM-electron energy-loss spectroscopy (EELS) mapping (Fig. 2e-h). It is clear that Pd_3Pb_1@Pd was composed of PdPb alloyed core with the unique atomic redistribution within the resultant PdPb aerogels, and the presence of a Pd shell around the PdPb core was indeed confirmed. Furthermore, the STEM-EELS line-scan in Fig. 2i and j also revealed the average thickness of Pd surface layer is about 0.5 ± 0.15nm (about three atomic layers), indicative of the evolution of the core-shell nanostructures.

Furthermore, the effect of Pd/Pb mole ratio on the gel formation was investigated. On the one hand, the molar ratio between Pd and Pb in the final aerogels can be tuned by controlling the precursor ratios (Table S1 and Fig. S2, ESI†). The gel formation can also be achieved within 4 hrs and no obvious difference was observed likely due to the accelerated gelation kinetics. The TEM images of the Pd_1Pb_1 (Fig. S3a, ESI†) and Pd_5Pb_1 (Fig. S3b, ESI†) revealed that these aerogels are also composed of irregularly fused nanoparticles. In contrast, the hydrogel can not be formed only in the presence of Pd precursor at least 12 h, demonstrating that the structure directing function of Pb plays a significant role in the formation of PbPb hydrogels. However, fused nanowire networks with narrow size distribution (~10 nm) for the Pd were also found (Fig. S3c, ESI†). The crystal structures of the as-prepared PdPb aerogels and monometallic Pd nanowire networks were further examined by X-ray powder diffraction (XRD) (Fig. 3a). Monometallic Pd nanowire networks exhibited a typical face-centered cubic (fcc) structure agreed well with a standard Pd pattern (JCPDS 46-1043). Upon addition of Pb, these PdPb@Pd aerogels are mainly composed of ordered Pd_3Pb intermetallic phase (JCPDS 20-0827) and a small negative shift in diffraction peaks was found with the increase in Pb content. As far as we know, it is also the first time for the synthesis of ordered intermetallic nanostructures in aqueous solution at very low temperature.[23-26] Meanwhile, it is noted that some weak diffraction peaks located at about 30° appeared for Pd_1Pb_1@Pd, which is likely due to the generation of Pb or Pb oxides within PdPt aerogels.[27] The overall Pd/Pb compositions, measured by inductively coupled plasma atomic emission spectroscopy (ICP-MS) are 54/46, 62/38 and 74/26 for Pd_1Pb_1, Pd_3Pb_1 and Pd_5Pb_1, respectively. The X-ray photoelectron spectroscopy (XPS) was also used to study the surface chemical composition and valence states (Figure S4a). Based on the XPS result, the atomic ratio of the different element was calculated and listed in Table. S2. In detail, Pd/Pb mole ratios are 64/36, 71/29, 79/21 for Pd_1Pb_1, Pd_3Pb_1 and Pd_5Pb_1, respectively, which were higher than those of ICP results and verified the Pd-enriched shell structures mentioned above. Both Pd and Pb in the Pb_3Pb_1 aerogel exhibited metallic state and oxide state (Fig. 3b). Trace amount P (3-6at%) was observed for PdPb aerogels likely because of the adsorption of P precursor and the phosphorus formed during the reduction process (Fig. S4b, ESI†). Noted that the P content can reach up to 30at% for Pd nanowire networks, revealing that P is more preferred to be evolved only in the presence of Pd precursor.

Based on the structure and composition features mentioned above, it can come to the conclusion that the introduction of sodium hypophosphite plays a dominated role in the evolution of the final hydrogels/aerogels. Accordingly, the related mechanism was proposed. Hypophosphite can reduce Pd^{2+} precursor to generate metallic Pd nuclei (Eq. 1).[28] Based on the fact that no obvious change was found when only Pb^{2+} existed in the precursor solution, it was proposed that Pb^{2+} was apt to be reduced in the presence of previously formed Pd nuclei (Eq. 2). On the one hand, the introduction Pb^{2+} accelerated gelation kinetics and directed the evolution of the core-shell PdPb@Pd hydrogels/aerogels with multiply-twinned defects. A large number of fused nanoparticles can be obviously observed in a very short time of ca. 30 s. On the other hand, different from the Pd nanowire networks enriched in P, it seems that the presence of Pb^{2+} inhibits the formation of P according to Eq. 3 and 4.[28, 29]

$$Pd^{2+} + H_2PO_2^- + 2OH^- \rightarrow Pd + H_2PO_3^- + H_2O \quad (1)$$

$$Pb^{2+} + H_2PO_2^- + 2OH^- \xrightarrow{Pd} Pb + H_2PO_3^- + H_2O \quad (2)$$

$$H_2PO_2^- + H^+ + H \rightarrow 2H_2O + P \quad (3)$$

$$H_2PO_2^- + 2H^+ + H^- \rightarrow 2H_2O + \frac{1}{2}H_2 + P \quad (4)$$

As a comparison, we also prepared PdPb hydrogels using $NaBH_4$ as reducing agent in spite of the relatively lower gelation kinetics. The TEM image in Fig. S5 (ESI†) shown a typical nanowire network with a diameter of about 8 nm, similar with PdCu aerogels reported previously.[18] The hypophosphite promotes the gelation in spite of the different fused nanostructures, which was ascribed to the less tendency of orientated attachment of building blocks because of the complex interaction among them. Despite the difference in standard reduction potential between $PdCl_4^{2+}$/Pd (+0.591 V vs standard hydrogen electrode (SHE)) and Pb^{2+}/Pb (-0.126 V vs RHE), Pd overlayer shell rather than Pb-enriched shell was formed,[30] which was closely associated with a rearrangement of dissimilar atoms driven by interdiffusion and segregation during the fusion of the nanoparticles at the early stage of the hydrogel formation.[31] The accelerated gelation kinetics has the other clear implication: The increase reaction temperature facilitates the orientated attachment of the unstable intermediate state and the fusion of the bare building blocks without capping agents was also favorable because of the high surface energy.[14, 30, 32] In contrast, the PdPb hydrogels can not be evolved at room temperature within 12 h. However, the powerful function of hypophosphite for evolving core-shell

PdPb@Pd with multiply-twinned grains and ordered

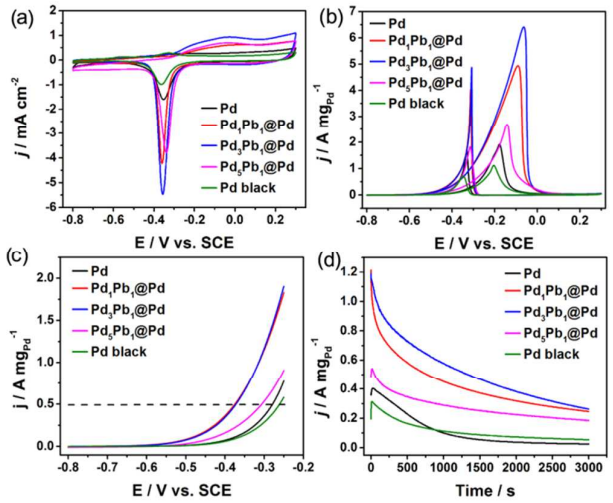

Fig. 4 CV curves of PdPb@Pd aerogels with different compositions, Pd and Pd black electrodes in aqueous N_2-saturated (a) 1 M KOH and (b) 1 M KOH + 0.5 M ethylene glycol solution at a scan rate of 50 mV s^{-1}. Current densities in (a) were normalized to the geometric electrode surface area. (c) Linear sweep voltammetry curves of different catalysts mentioned above 1 M KOH + 0.5 M ethylene glycol solution at a scan rate of 50 mV s^{-1}. (d) Current density–time curves of aforementioned electrocatalysts in 1 M KOH + 0.5 M ethylene glycol solution at –0.3 V.

intermetallic phase is still needed to be investigated. Another important feature of hypophosphite is the high selectivity towards the reduction of noble metal precursors. Although the higher standard reduction potential of $PtCl_6^{2+}$/Pt (0.742 V vs RHE) and $AuCl_4^-$/Au (1.002 V vs RHE) than that of $PdCl_4^{2+}$/Pd, no color change was found when hypophosphite was added to the Au and Pt involved precursor solutions (Fig. S6, ESI†). However, we found the Cu^{2+} had the same function and successfully extend this synthetic approach to PdCu hydrogels/aerogel with different compositions (Fig. S7, ESI†). Taken together, hypophosphite reduction provided a promising alternative route for the construction of more complex noble metal-based aerogel at the nanoscale via one-step approach, holding great promise for different applications.

The use of ethylene glycol (EG) in direct alcohol fuel cells has gained great interest and Pd-based nanomaterials have demonstrated superior electrocatalytic activity for EG oxidation reaction (EGOR) in alkaline media.[33-38] Taking advantage of the porous feature, ordered intermetallic phase, bare surface as well as core-shell nanostructures with multiply-twinned defects, the resultant bimetallic PdPb@Pd aerogels are expected to be good candidates for EGOR in alkaline solution. First, the cyclic voltammetry (CV) curves of PdPb aerogels, Pd nanowire network and Pd black were recorded in 1 M KOH at a sweep rate of 50 mV s^{-1}. By quantification of the electric charges associated with the reduction of PdO, the electrochemically active surface areas (ECSAs) of Pd nanowire network, Pd_1Pb_1@Pd aerogel, Pd_3Pb_1@Pd aerogel, Pd_5Pb_1@Pd aerogel and Pd black are determined to be 20.6, 28.3, 41.8, 30.5 and 12.9 m^2 g^{-1}, respectively. The electrocatalytic properties of PdPb@Pd aerogels towards EGOR have been subsequently investigated in 1 M KOH + 0.5 M EG at a scan rate of 50 mV s^{-1}. As shown in Figure 4b and c, compared with monometallic Pd nanowire networks and Pd black, the electrocatalytic activities of PdPb@Pd aerogels in term of the peak currents and onset potentials were significantly improved, demonstrating the structural and compositional advantage of the resultant bimetallic aerogels. Among these catalysts, Pd_3Pb_1@Pd aerogels not only had the largest ECSA but also exhibited the lowest onset potential and highest mass activity. Specifically, the mass activity of Pd_3Pb_1@Pd aerogels can reach to 6.4 A mg_{Pd}^{-1}, which is about 1.3, 2.4, 3.4 and 5.8 times that of Pd_1Pb_1@Pd, Pd_5Pb_1@Pd, Pd nanowire networks and Pd black, respectively. Moreover, this value is also considerably higher than that of Pd-based catalysts reported previously (Table S3). Furthermore, the stability of the PdPb@Pd aerogels for EGOR was examined by chronoamperometric experiments. The current-time curves in Fig. 4d clearly verified the fact that the introduction of Pb is of great significance for the enhanced stability and all the PdPb@Pd aerogels have a better stability than monometallic counterparts. As expected, Pd_3Pb_1@Pd aerogels possessed the highest current density among these catalysts over the whole 3000 s test. Besides, ICP-MS measurement showed that no distinct Pb (< 0.002 ug/L) was leaked out from catalysts after long stability test (50000s), indicating the structural stability of the Pd_3Pb_1@Pd.

Conclusions

In summary, using sodium hypophosphite as a functional reducing agent, we succeeded in synthesizing core-shell PdPb@Pd aerogels with multiply-twinned defects through one-step method. In addition to the specific function of hypophosphite, the accelerated gelation kinetics can be realized simply through increasing reaction temperature and the formation of this kind of hydrogels can be completed with 4 hrs. Benefitting from the unique 3D porous characteristics, bare surface and the favorable geometric and electronic synergy including ordered intermetallic phase and controlled core-shell structures with multiply-twinned grains, the PdPb@Pd aerogels reported herein exhibited high electrocatalytic activity and stability toward EGOR. The mass activity of the optimized Pd3Pb1@Pd aerogels is about 5.8 times higher than that of Pd black. This study provides a new structure and composition-engineering strategy for designing more functional noble metal-based aerogels with an excellent electrocatalytic performance for EGOR and beyond.

Conflicts of interest

There are no conflicts to declare.

Acknowledgements

This work was supported by a start-up fund of Washington State University, USA. The XPS analysis was performed using EMSL, a national scientific user facility sponsored by the

Department of Energy's Office of Biological and Environmental Research and located at Pacific Northwest National Laboratory (PNNL). Part of electron microscopy work was performed at the Center for Functional Nanomaterials, Brookhaven National Laboratory, which is supported by the U.S. Department of Energy (DOE), Office of Basic Energy Science, under contract DE-SC0012704. The authors also acknowledge Franceschi Microscopy and Image Center at Washington State University for TEM measurements. PNNL is a multiprogram national laboratory operated for DOE by Battelle under Contract DEAC05-76RL01830. The authors would like to thank Dr. Indranil Chowdhury at WSU for ICP-MS measurement.

Notes and references

1 C. Li, Ö. Dag, T. D. Dao, T. Nagao, Y. Sakamoto, T. Kimura, O. Terasaki and Y. Yamauchi, *Nat Commun*, 2015, **6**, 6608.
2 B. Lim, M. Jiang, P. H. C. Camargo, E. C. Cho, J. Tao, X. Lu, Y. Zhu and Y. Xia, *Science*, 2009, **324**, 1302-1305.
3 C. Zhu, D. Du, A. Eychmüller and Y. Lin, *Chem. Rev.*, 2015, **115**, 8896-8943.
4 V. Malgras, H. Ataee-Esfahani, H. Wang, B. Jiang, C. Li, K. C. W. Wu, J. H. Kim and Y. Yamauchi, *Adv. Mater.*, 2016, **28**, 993-1010.
5 K. S. Krishna, C. S. S. Sandeep, R. Philip and M. Eswaramoorthy, *ACS Nano*, 2010, **4**, 2681-2688.
6 K. Liu, Y. Bai, L. Zhang, Z. Yang, Q. Fan, H. Zheng, Y. Yin and C. Gao, *Nano Lett.*, 2016, **16**, 3675-3681.
7 W. Liu, A.-K. Herrmann, N. C. Bigall, P. Rodriguez, D. Wen, M. Oezaslan, T. J. Schmidt, N. Gaponik and A. Eychmüller, *Acc. Chem. Res.*, 2015, **48**, 154-162.
8 D. Wen, W. Liu, D. Haubold, C. Zhu, M. Oschatz, M. Holzschuh, A. Wolf, F. Simon, S. Kaskel and A. Eychmüller, *ACS Nano*, 2016, **10**, 2559-2567.
9 N. C. Bigall, A.-K. Herrmann, M. Vogel, M. Rose, P. Simon, W. Carrillo-Cabrera, D. Dorfs, S. Kaskel, N. Gaponik and A. Eychmüller, *Angew. Chem., Int. Ed.*, 2009, **48**, 9731-9734.
10 Q. Shi, C. Zhu, Y. Li, H. Xia, M. H. Engelhard, S. Fu, D. Du and Y. Lin, *Chem. Mater.*, 2016, **28**, 7928-7934.
11 W. Liu, D. Haubold, B. Rutkowski, M. Oschatz, R. Hübner, M. Werheid, C. Ziegler, L. Sonntag, S. Liu, Z. Zheng, A.-K. Herrmann, D. Geiger, B. Terlan, T. Gemming, L. Borchardt, S. Kaskel, A. Czyrska-Filemonowicz and A. Eychmüller, *Chem. Mater.*, 2016, **28**, 6477-6483.
12 B. Cai, A. Dianat, R. Hübner, W. Liu, D. Wen, A. Benad, L. Sonntag, T. Gemming, G. Cuniberti and A. Eychmüller, *Adv. Mater.*, 2017, **29**, 1605254.
13 B. Cai, D. Wen, W. Liu, A.-K. Herrmann, A. Benad and A. Eychmüller, *Angew. Chem., Int. Ed.*, 2015, **54**, 13101-13105.
14 A.-K. Herrmann, P. Formanek, L. Borchardt, M. Klose, L. Giebeler, J. Eckert, S. Kaskel, N. Gaponik and A. Eychmüller, *Chem. Mater.*, 2014, **26**, 1074-1083.
15 X. Gao, R. J. Esteves, T. T. H. Luong, R. Jaini and I. U. Arachchige, *J. Am. Chem. Soc.*, 2014, **136**, 7993-8002.
16 W. Liu, A.-K. Herrmann, D. Geiger, L. Borchardt, F. Simon, S. Kaskel, N. Gaponik and A. Eychmüller, *Angew. Chem., Int. Ed.*, 2012, **51**, 5743-5747.
17 W. Liu, P. Rodriguez, L. Borchardt, A. Foelske, J. Yuan, A.-K. Herrmann, D. Geiger, Z. Zheng, S. Kaskel, N. Gaponik, R. Kötz, T. J. Schmidt and A. Eychmüller, *Angew. Chem., Int. Ed.*, 2013, **52**, 9849-9852.
18 C. Zhu, Q. Shi, S. Fu, J. Song, H. Xia, D. Du and Y. Lin, *Adv. Mater.*, 2016, **28**, 8779-8783.
19 S. Henning, L. Kühn, J. Herranz, M. Nachtegaal, R. Hübner, M. Werheid, A. Eychmüller and T. J. Schmidt, *Electrochim. Acta*, 2017, **233**, 210-217.
20 H. Mistry, A. S. Varela, S. Kühl, P. Strasser and B. R. Cuenya, *Nat. Rev. Mater.*, 2016, **1**, 16009.
21 J. Wu, L. Qi, H. You, A. Gross, J. Li and H. Yang, *J. Am. Chem. Soc.*, 2012, **134**, 11880-11883.
22 X. Sun, K. Jiang, N. Zhang, S. Guo and X. Huang, *ACS Nano*, 2015, **9**, 7634-7640.
23 Y. Yan, J. S. Du, K. D. Gilroy, D. Yang, Y. Xia and H. Zhang, *Adv. Mater.*, 2017, **29**, 1605997.
24 J. Kim, Y. Lee and S. Sun, *J. Am. Chem. Soc.*, 2010, **132**, 4996-4997.
25 S. Maksimuk, S. Yang, Z. Peng and H. Yang, *J. Am. Chem. Soc.*, 2007, **129**, 8684-8685.
26 K. Jiang, P. Wang, S. Guo, X. Zhang, X. Shen, G. Lu, D. Su and X. Huang, *Angew. Chem., Int. Ed.*, 2016, **55**, 9030-9035.
27 P. Wu, Y. Huang, L. Zhou, Y. Wang, Y. Bu and J. Yao, *Electrochim. Acta*, 2015, **152**, 68-74.
28 K. Wu, X. Mao, Y. Liang, Y. Chen, Y. Tang, Y. Zhou, J. Lin, C. Ma and T. Lu, *J. Power Sources*, 2012, **219**, 258-262.
29 L. Zhang, D. Lu, Y. Chen, Y. Tang and T. Lu, *J. Mater. Chem. A*, 2014, **2**, 1252-1256.
30 C. Zhu, D. Wen, M. Oschatz, M. Holzschuh, W. Liu, A.-K. Herrmann, F. Simon, S. Kaskel and A. Eychmüller, *Small*, 2015, **11**, 1430-1434.
31 L. Kühn, A.-K. Herrmann, B. Rutkowski, M. Oezaslan, M. Nachtegaal, M. Klose, L. Giebeler, N. Gaponik, J. Eckert, T. J. Schmidt, A. Czyrska-Filemonowicz and A. Eychmüller, *Chem. Eur. J.*, 2016, **22**, 13446-13450.
32 H.-G. Liao, L. Cui, S. Whitelam and H. Zheng, *Science*, 2012, **336**, 1011-1014.
33 L. An and R. Chen, *J. Power Sources*, 2016, **329**, 484-501.
34 C. Bianchini and P. K. Shen, *Chem. Rev.*, 2009, **109**, 4183-4206.
35 W. Hong, C. Shang, J. Wang and E. Wang, *Energy Environ. Sci.*, 2015, **8**, 2910-2915.
36 S. Li, J. Lai, R. Luque and G. Xu, *Energy Environ. Sci.*, 2016, **9**, 3097-3102.
37 P. Wu, Y. Huang, L. Kang, M. Wu and Y. Wang, *Sci. Rep.*, 2015, **5**, 14173.
38 Y. Feng, L. Bu, S. Guo, J. Guo and X. Huang, *Small*, 2016, **12**, 4464-4470.

TOC Figure